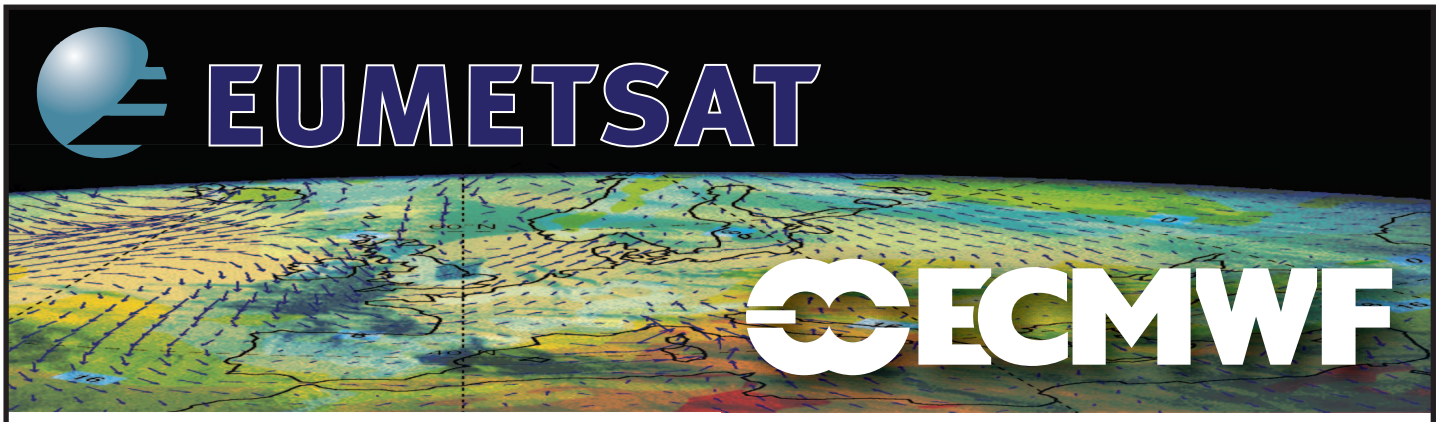

EUMETSAT/ECMWF Fellowship Programme
Research Report No. 29

Assimilation of ATOVS radiances at ECMWF: third year EUMETSAT fellowship report

E. Di Tomaso, N. Bormann and S. English

August 2013

Series: EUMETSAT/ECMWF Fellowship Programme Research Reports

A full list of ECMWF Publications can be found on our web site under:
http://www.ecmwf.int/publications/

Contact: library@ecmwf.int

European Centre for Medium Range Weather Forecasts
Shinfield Park, Reading, RG2 9AX, England

1 Executive summary

This report summarises work towards enhancing the usage of satellite microwave observations in the ECMWF system. Observations from the ATOVS microwave (MW) sounders, AMSU-A and MHS, will be considered in these studies. Three topics will be discussed: the evaluation of new instruments, the enhancement of observations at high latitudes and the characterisation of an error model for observations sensitive to the surface. The main results are summarised here for the three different topics.

In the first part of the report, we describe the assessment of the quality of AMSU-A and MHS data onboard the recently launched Metop-B satellite, prior to their active assimilation in the ECMWF system. Scan-dependent statistics (in terms of bias and standard deviation of FG-departures) showed promptly that the two instruments were, from the start, in a very healthy condition, and the instrument noise compared well to the one of the twin sensors onboard the Metop-A satellite.

Metop-B AMSU-A and MHS have been monitored passively in operations (i.e. without having a weight on the estimation of the atmospheric analysis) prior to their active assimilation, allowing the spin-up of the variational bias correction (VarBC) coefficients, and the monitoring of bias-corrected and quality-controlled data. The VarBC coefficients adjusted themselves to stable values within a few assimilation cycles, and data characteristics were stable after that.

We have run a set of assimilation experiments where the MW sounders from Metop-B were actively assimilated in our system. The position and timing of the Metop-B orbit allows for most of the data to be selected by our thinning scheme. The assimilation of Metop-B MW sounders brings an improvement to the fit of MHS and ATMS data already present in the system, and the assimilation trials show a positive forecast impact in the short-term from adding Metop-B MW sounders to the operational suite of observations. AMSU-A channel 7 (which is malfunctioning on Metop-A AMSU-A) plays a role in the positive impact that these sensors have in the Northern Hemisphere. Consistent with the NOAA-19 and ATMS experience, we are still seeing improvements from adding MW data in our system.

As result of these studies, the two Metop-B microwave sounders have been actively assimilated at ECMWF since 10 December 2012.

In the second part of the report, we describe an enhancement of the assimilation of AMSU-A and MHS at high latitudes through a better specification of the surface emissivity. For AMSU-A this has involved improving the assimilation of observations already active over sea ice, while for MHS currently unused observations over sea and sea ice were considered for assimilation at high latitudes. This work was built on the preliminary results obtained by low resolution experiments (at T319) that have been reported in the second year fellowship report.

To improve the specification of the surface emissivity over sea ice, we adapt the dynamic emissivity scheme currently used over land for AMSU-A and MHS. In this scheme the emissivity for the sounding channels is retrieved using observations from a window channel. For AMSU-A, we applied the same scheme that is used over land also over sea ice: AMSUA sounding channels are close enough in frequency to the emissivity channel such that a frequency parameterisation is not necessary. For MHS, the scheme needed to be modified for sea ice, due to significant emissivity variations with frequencies. For both sensors the dynamic emissivities lead to improved simulations for the actively simulated channels, and, as a consequence, an increased number of microwave sounder observations are assimilated at high latitudes. This is the case for MHS channel 3 and 4, but also for AMSU-A channel 5 to 8.

The trial assimilation runs in the summer season show a positive impact for the forecast of the temperature, geopotential and winds in the Southern Hemisphere, and an impact mainly neutral elsewhere. The winter experiments show a positive impact for the relevant atmospheric variables in both hemispheres, which is in agreement with changes in the temperature and humidity analysis fields that occur both in the North and South Polar region.

The changes at high latitudes for AMSU-A and MHS described in this report will be implemented at ECMWF in the next cycle upgrade (CY39R1).

In the last part of the report, we describe a surface-dependent observation error model for AMSU-A channel 5, the lowest peaking channel among the actively assimilated AMSU-A channels at ECMWF. This error model takes into account both the observation sensitivity to the surface and the emissivity errors. Our uncertainty about the surface description varies in fact with surface type. Furthermore, measurements taken in a certain frequency range (or channel) have a different sensitivity to the surface depending on the scanning angle: observations at outer scan positions are less sensitive to the surface than nadir ones as the atmospheric path increases away from nadir.

We have estimated an observation error which is dependent on the channel transmittance from surface to space and on the type of surface observed (high vegetation, low vegetation, desert/semidesert, snow, sea ice and sea). The estimated observation errors are smaller than what is currently used in operations for AMSU-A channel 5 near the scan edge, and are bigger (with the exception of sea surfaces) for observations near nadir.

Assimilation trials show a neutral impact from changing the observation error from the currently used value of 0.28 (globally constant). However, this study provides an initial base for future work towards a more efficient usage of surface-dependent observations.

2 Metop-B Initial assessment

EUMETSAT has started the trial dissemination of AMSU-A and MHS Level 1B products from the Metop-B satellite respectively on 28 September and on 2 October 2012. The two microwave sounders come to join a family of five AMSU-A, three MHS and one ATMS sensor currently assimilated in our system. This is indeed a data-rich period for the MW sounders. However, previous studies have shown that a configuration of six AMSU-A and four AMSU-B/MHS instruments outperforms other constellations where less MW sounder sensors are assimilated (Di Tomaso and Bormann 2011).

Furthermore, the position and timing of the Metop-B orbit allows for most of the data to be selected by our thinning scheme. Figure 1 shows some examples of a 30 minute coverage for the AMSU-A sensors currently considered for assimilation. The AMSU-A data onboard different satellites within each 30 minute window are thinned together in our system to avoid over-sampling and spatial correlation of the observation errors (spatial correlation is not taken into account in the current representation of the observation error). A similar thinning procedure is applied also to the MHS sensors.

Figure 2 and 3 show scan-dependent statistics (in terms of bias and standard deviation of FG-departures) for Metop-A and Metop-B calculated for the first Metop-B data received by EUMETSAT on 26 September 2012 (two orbits for AMSU-A and one orbit for MHS), and nearly simultaneous Metop-A observations. Only data over sea were considered in the calculations, and after some quality control to remove cloud/rain contamination in the lower channels. Possible sampling issues might be affecting these values that were calculated with such a small set of data, however, these first results showed promptly that the instruments were from the start both in a very healthy condition, and the instrument noise compared well to the one of Metop-A. Subsequent longer-term monitoring confirmed these initial results.

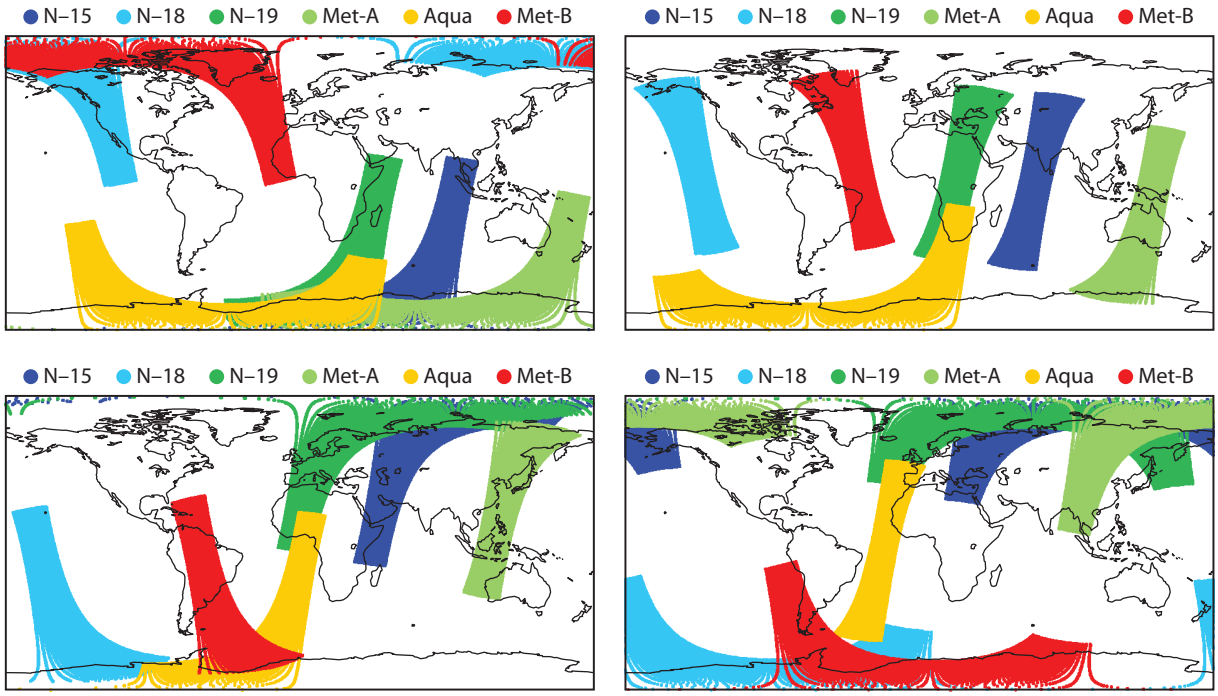

Figure 1: Examples of a 30 minute coverage of the six AMSU-A sensors onboard NOAA-15, NOAA-18, NOAA-19, Metop-A, Aqua and Metop-B.

Metop-B AMSU-A and MHS have been monitored passively in operations (i.e. without having a weight on the estimation of the atmospheric analysis) since 4 October 2012, allowing the spin-up of the variational bias correction (VarBC) coefficients, and the monitoring of bias-corrected and quality-controlled data. Figures 4 and 5 show for example the global first-guess departure statistics for AMSU-A channel 8 and MHS channel 3 that were published online for the first month and half of monitoring of the data (Microwave Instruments 2012). The VarBC coefficients adjusted themselves to stable values within a few assimilation cycles, and data characteristics appear stable after this.

2.1 Assimilation experiment setup

In this section we evaluate the benefit of assimilating the Metop-B MW sounders on top of all observations currently used in operations, or as a replacement of Metop-A MW sounders. We have run a set of assimilation experiments where the MW sounders from Metop-B were actively assimilated in our system as follows:

- 'MetB' experiment: This experiment adds to the full operational capability the assimilation of Metop-B AMSU-A and MHS;
- 'MetB-MetA' experiment: This experiment is identical to the 'MetB' experiment except for the denial of the Metop-A MW sounders;
- 'MetB-ch7-MetA' experiment: This experiment is identical to the 'MetB-MetA' experiment except for the denial of channel 7 on Metop-B AMSU-A;
- 'CTL' experiment: This experiment uses the full operational observation capability.

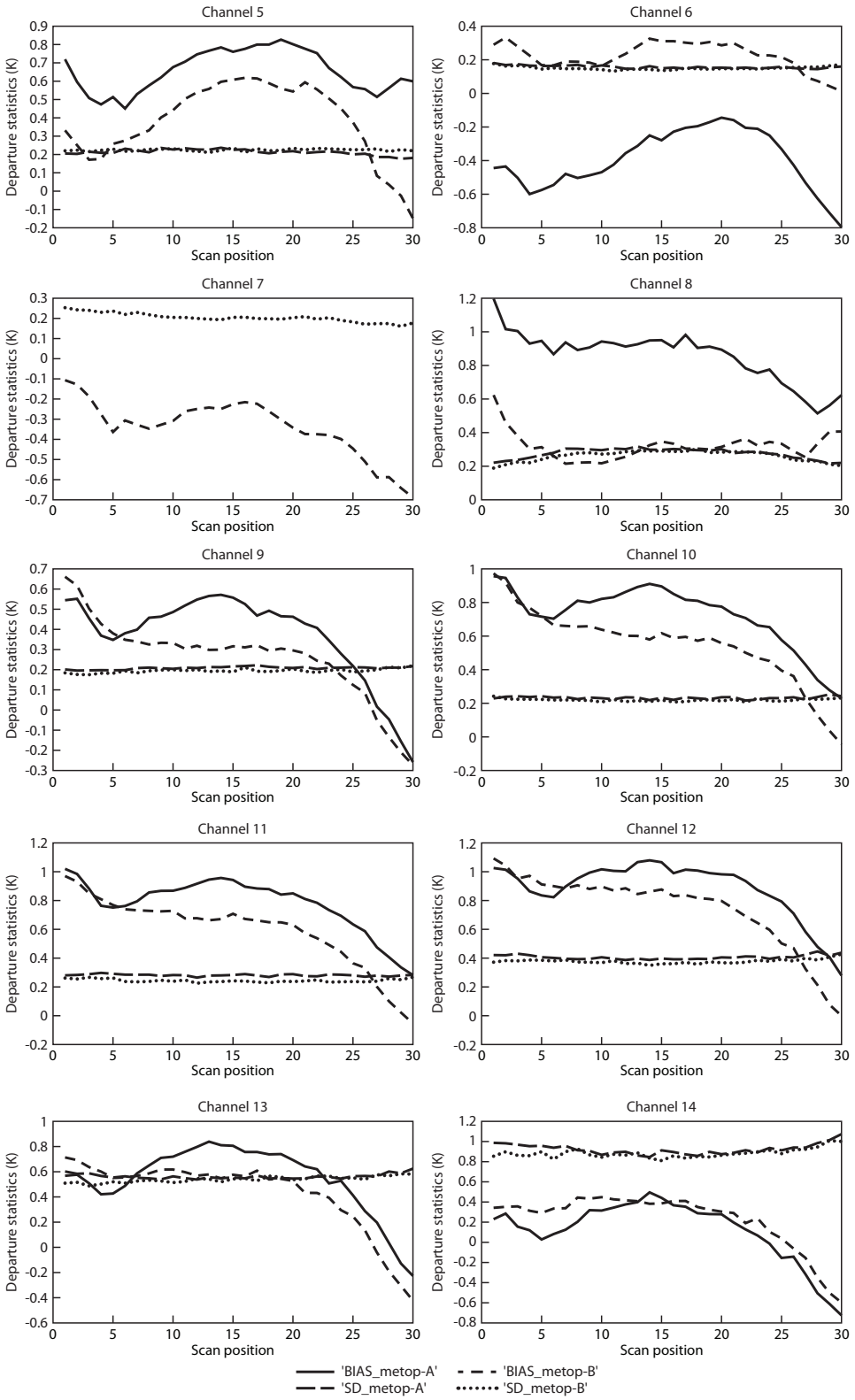

Figure 2: Scan-dependent statistics (in terms of bias and standard deviation of FG-departures) for Metop-A and Metop-B AMSU-A channel 5 to 14 calculated for two orbits of data on 26 September 2012 over sea and after some quality control based on first-guess checks applied to the lower channels. Note that channel 7 is malfunctioning on Metop-A.

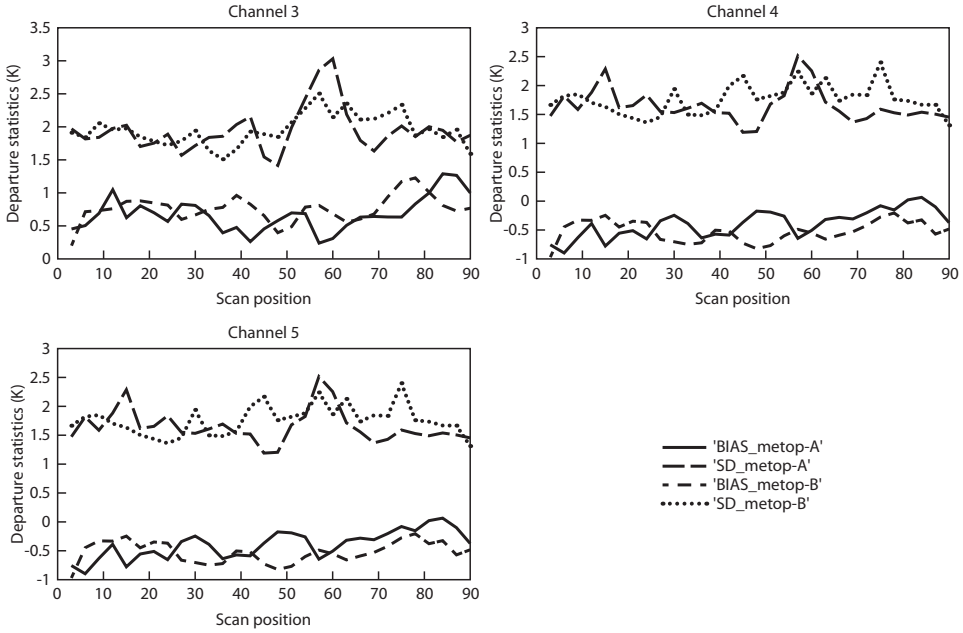

Figure 3: Scan-dependent statistics (in terms of bias and standard deviation of FG-departures) for Metop-A and Metop-B MHS channel 3 to 5 calculated for one orbits of data on the 26 September 2012 over sea and after some quality control based on a scattering index applied to remove cloud/rain contamination.

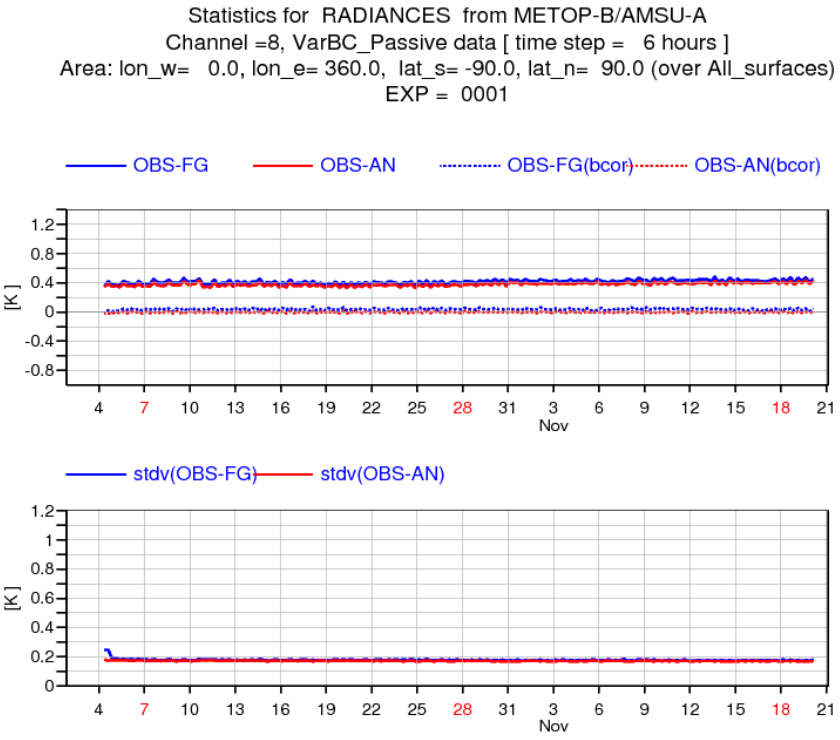

Figure 4: MetOp-B AMSU-A channel 8 brightness temperature departure statistics for data monitored passively from 4 October 2012.

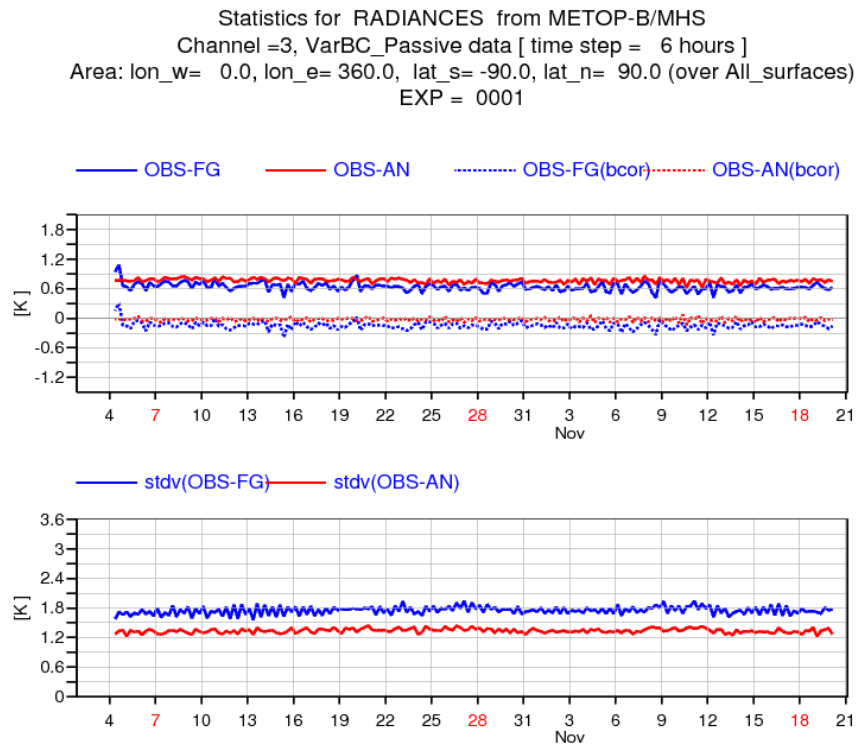

Figure 5: MetOp-B MHS channel 3 brightness temperature departure statistics for data monitored passively from 4 October 2012.

The 'MetB' experiment aims to assess the impact of adding the Metop-B MW sounders in our current system, while the 'MetB-MetA' experiment simulates a swap between Metop-A and Metop-B for the MW sounders. The comparison between the 'MetB-MetA' experiment and the 'MetB-ch7-MetA' experiment aims to assess the contribution of AMSU-A channel 7 to any potential benefit coming from assimilating the Metop-B MW sensors (AMSU-A on Metop-A is having a malfunctioning channel 7 since about two years from its launch).

The Metop-B sensors are treated like the equivalent sensors already assimilated and flying on other platforms. For example they are thinned to a resolution of 125 km in a 30 minute window, and are quality controlled for rain/cloud contamination with checks on the first-guess departures of passive window channels. Surface sensitive channels are screened on surfaces which are particularly difficult to model: high orography, snow and sea ice. The emissivity over land is calculated using the FASTEM scheme (Liu et al. 2011), and over land emissivities are dynamically retrieved from window channel observations and first-guess model fields (Karbou et al. 2005). The observation error is a global constant per channel, and it is not platform-dependent.

The above assimilation experiments were run at a T511 resolution and with cycle CY38R1 from 16 October 2012 to 9 December 2012.

2.2 Results

2.2.1 Departure statistics of the first guess and analysis

The impact of the Metop-B AMSU-A and MHS data on the quality of the analysis and of the first guess is assessed here by studying the fit to conventional and satellite observations. Both background (first guess)

departure statistics and analysis departure statistics are calculated after the bias correction of satellite radiances.

There are no relevant differences in the departure statistics of the radiosonde observations that can be attributed to the assimilation of Metop-B MW sensors.

The assimilation of Metop-B MW sounders brings a small improvement to the fit of MHS and ATMS data already present in the system. The improvement is shown in terms of a small reduction in the standard deviation of first-guess departures together with a small increase in the data count of assimilated observations. Figure 6 shows for example the fit to Metop-A MHS in the Northern Hemisphere. Similar results are also obtained for the Southern Hemisphere and the Tropics, and for the other MHS sensors on board of NOAA-18 and NOAA-19. Also the fit to the humidity sounding channels of ATMS (i.e. channels 18 to 22) improves with the assimilation of Metop-B AMSU-A and MHS (see Figure 7). A small reduction in the number of used AMSU-A and MHS data for other satellites than Metop-A is observed in the polar regions. This is due to the combined thinning of the sensors in these areas.

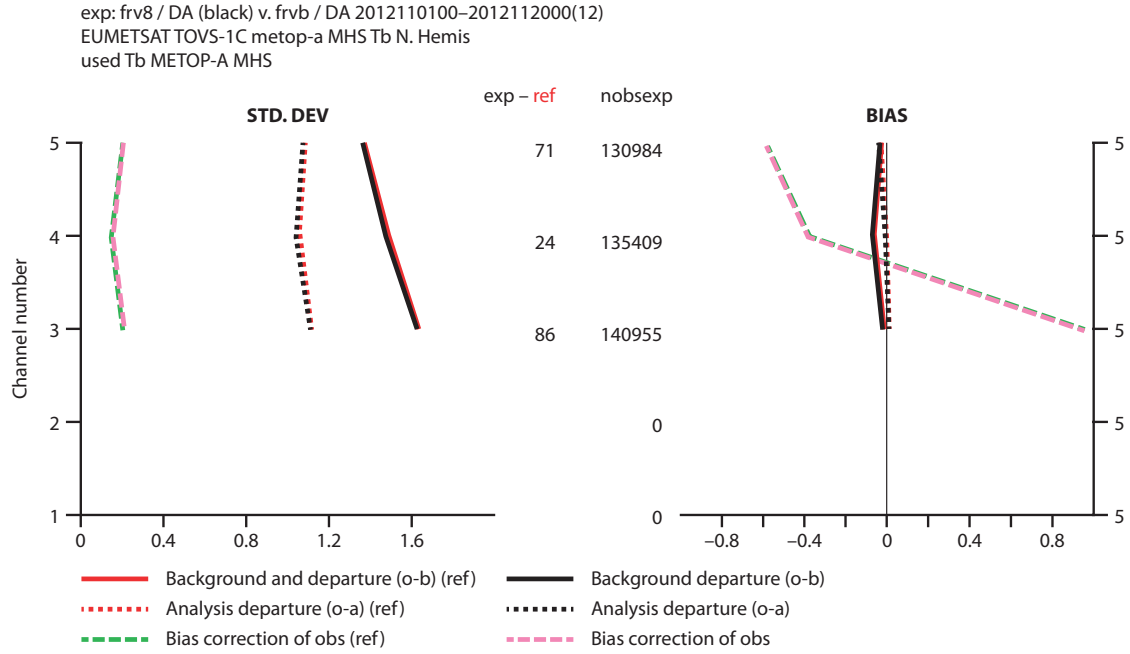

Figure 6: MetOp-A MHS brightness temperature departure statistics for the 'MetB' experiment (frv8) (black) and the 'CTL' experiment (frvb) (red) for the Northern Hemisphere.

2.2.2 Forecast impact

We have studied the experiments' impact on the forecast for different variables, regions and forecast ranges, computing forecast results for 55 days of assimilation experiments over the period 16 October 2012 to 9 December 2012.

Zonal means of the forecast error differences for the geopotential show a positive impact in the short range from adding Metop-B MW sounders to the operational suite of observations (see figure 8). The impact is statistically significant in the extra-Tropics up to the first day of the forecast.

Figure 9 shows the differences in the root mean squared forecast error between the three experiments ('MetB', 'MetB-MetA, and 'MetB-ch7-MetA) and the control averaged over the Southern Hemisphere, the Tropics and the Northern Hemisphere. The impact of the 'MetB-MetA' experiment is comparable to the one of the 'MetB'

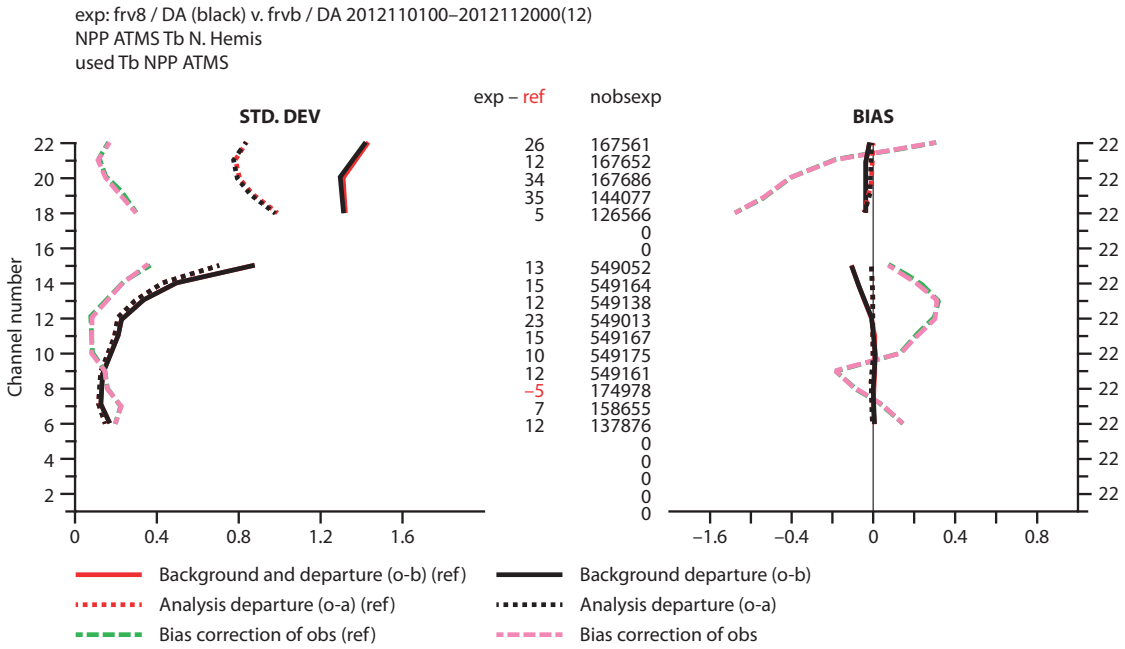

Figure 7: ATMS brightness temperature departure statistics for the 'MetB' experiment (frv8) (black) and the 'CTL' experiment (frvb) (red) for the Northern Hemisphere.

experiment (i.e. significantly positive in the short term, neutral elsewhere). The results of 'MetB-ch7-MetA' experiment show that AMSU-A channel 7 on Metop-B indeed plays a role in the positive impact of the 'MetB' experiment in the Northern Hemisphere in the short-term (without channel 7 this impact becomes neutral for the forecast of the geopotential at 500 hPa and 850 hPa).

For the forecast of the other atmospheric variables the impact of the three experiments versus the control is in general neutral, while a positive impact is observed for the forecast of the mean sea level pressure in the short range, consistent with the improvement in the geopotential forecast.

2.3 Conclusions

The quality of Metop-B MW sounder data has been evaluated through a comparison with simulated radiances from the model state. Statistics of first-guess departures for passive monitored data show that both AMSU-A and MHS sensors are in very healthy conditions.

We have also tested the active usage of the data in assimilation experiments run at a T511 resolution. The assimilation trials show a positive forecast impact in the short-term from adding Metop-B MW sounders to the operational suite of observations. As result of these studies the two Metop-B microwave sounders have been actively assimilated at ECMWF since 10 December 2012.

Consistent with the NOAA-19 and ATMS experience, we are still seeing improvements from adding MW data in our system. This is partly because the new sensors cover data gaps due to broken channels in the sensors already assimilated.

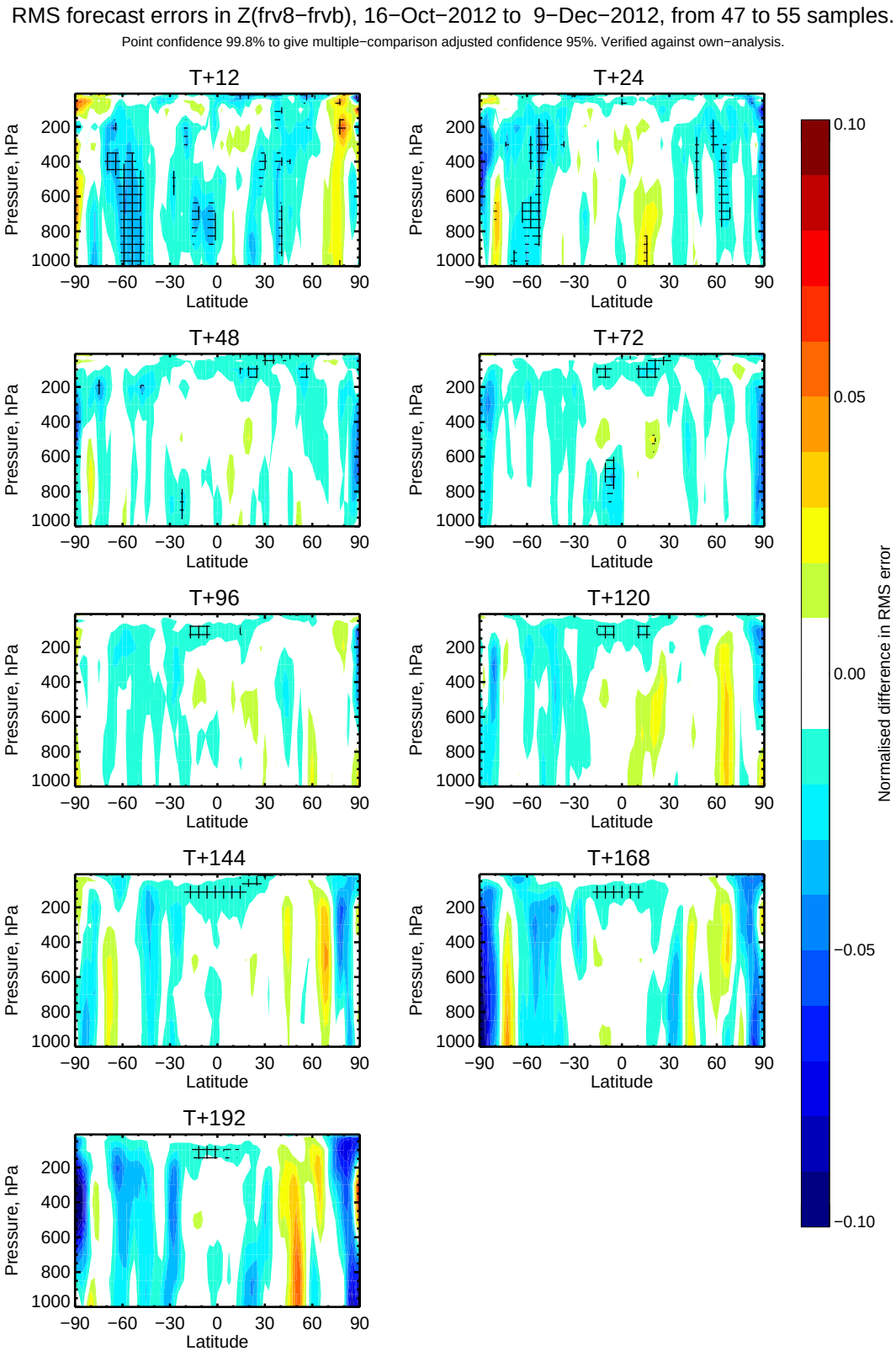

Figure 8: Zonal means of normalised differences in the root mean square forecast error for the geopotential between the 'MetB' experiment (frv8) and the 'CTL' experiment (frvb). Blue shading indicates an improvement in frv8 compared to frvb. Verification is against the experiment own-analysis.

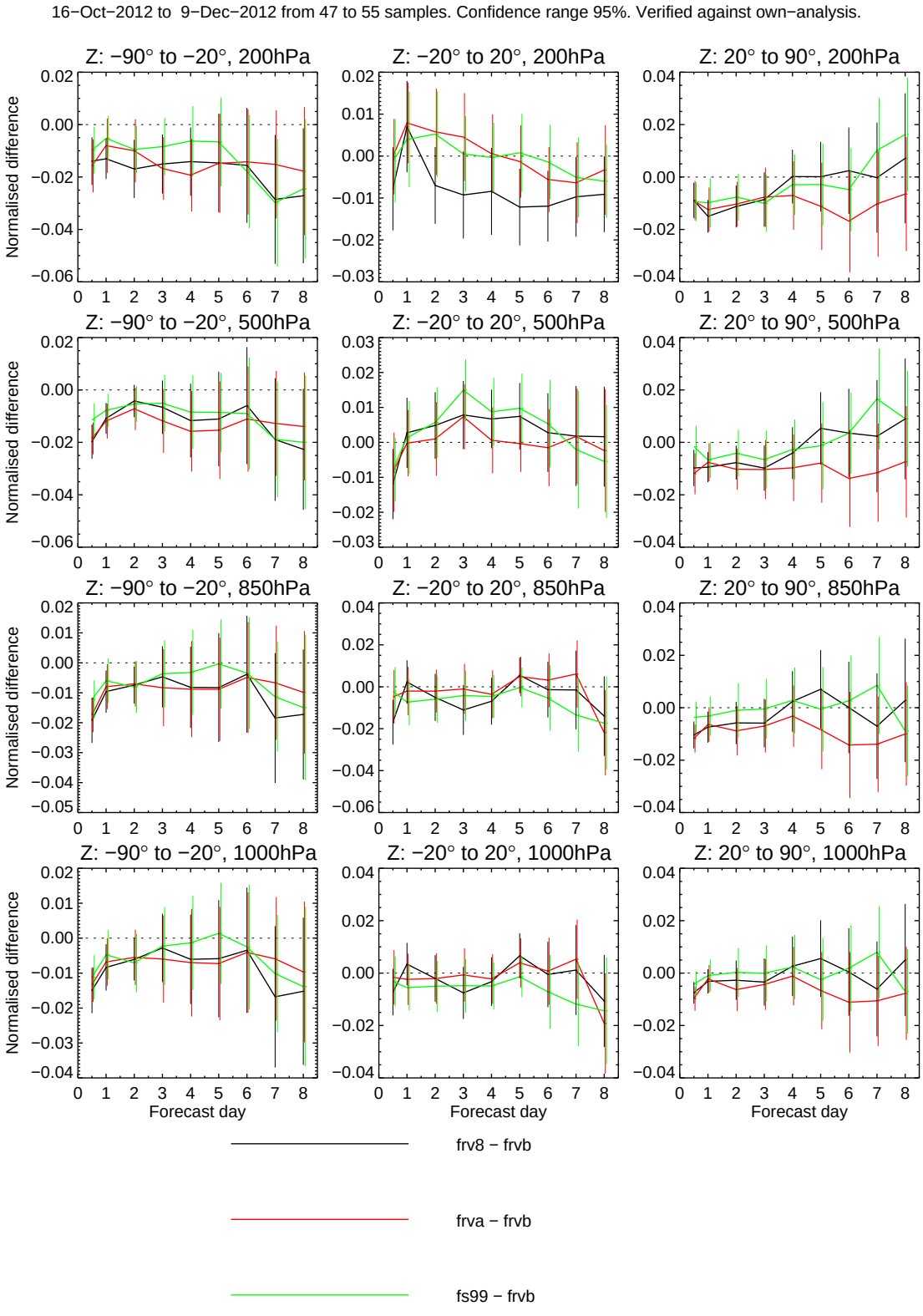

Figure 9: Normalised differences in the root mean square forecast error between the 'MetB' experiment (frv8) and the 'CTL' experiment (frvb) (black), between the 'MetB-MetA' experiment (frva) and the 'CTL' experiment (frvb) (red), and between the 'MetB-ch7-MetA' experiment (fs99) and the 'CTL' experiment (frvb) (green) for the 0Z forecast of the 200 hPa, 500 hPa, 850 hPa and 1000 hPa geopotential. Verification is against the experiment own-analysis.

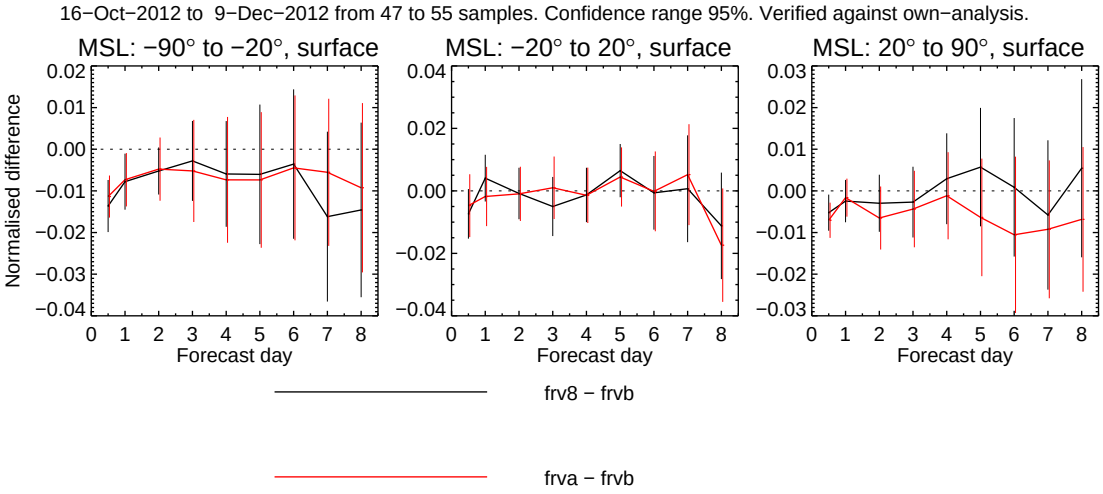

Figure 10: Normalised differences in the root mean square forecast error between the 'MetB' experiment (frv8) and the 'CTL' experiment (frvb) (black), and between the 'MetB-MetA' experiment (frva) and the 'CTL' experiment (frvb) (red) for the 0Z forecast of mean sea level pressure. Verification is against the experiment own-analysis.

3 Enhanced assimilation of microwave sounding data at high latitudes

Here we discuss work towards an operational enhancement of the assimilation of AMSU-A and MHS at high latitudes through a better specification of the surface emissivity. For AMSU-A this involves improving the assimilation of observations already assimilated over sea ice, while for MHS currently unused observations over sea and sea ice are considered for assimilation at high latitudes. This work is built on the preliminary results obtained with low resolution experiments (at T319) that have been reported in the second year fellowship report (Di Tomaso and Bormann 2012). The low resolution experiments have shown the benefit of using dynamic emissivities over sea ice. The dynamic retrieval of emissivities is based on re-arranging the radiative transfer equation for window channel observations and using the ECMWF model background field (Karbou et al. 2005). Here we report on studies performed at higher resolution (at T511), and give a more detailed analysis of the changes.

AMSU-A observations from channel 5 to 14 are assimilated operationally over low orography, sea and sea ice, but with channel 5 not active south of 60S. Other channels are either discarded or used for emissivity retrieval over land (channel 3 at 50.3 GHz), and quality control purposes over land (channel 4 at 52.8 GHz) and over sea (channel 3 at 50.3 GHz). Emissivities over sea ice for AMSU-A are calculated with a static scheme based on a classification of the surface type and an appropriate parametric model per surface type (Kelly and Bauer 2000).

MHS observations from channel 3, 4 and 5 (the 3 channels in the 183 GHz water vapour band) are assimilated operationally only over surfaces with skin temperature TS $>$ 278 K and over low orography. The constraint on the skin temperature means that there is no humidity sounding coverage in most areas polewards of 60 degrees which include sea ice. The other two MHS channels (namely window channels) are used for emissivity retrieval over land (channel 1 at 89 GHz) and quality control purposes (channel 2 at 157 GHz).

As shown also in Bouchard et al. 2010, and Di Tomaso and Bormann 2012, the dynamic retrieval of emissivities provides a good basis to improve the use of microwave sounding data over sea ice.

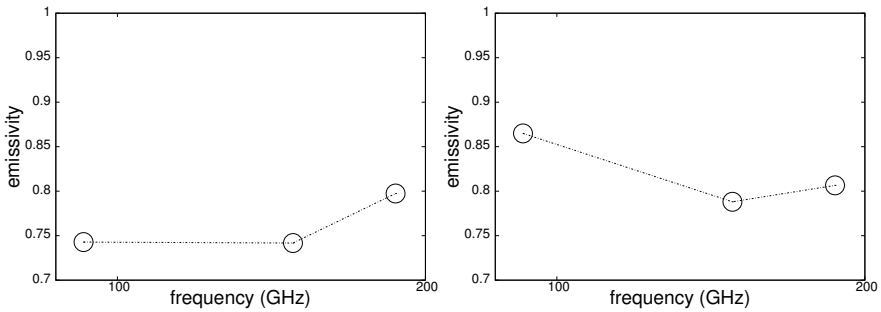

Figure 11: Emissivity spectra for two different types of sea ice, where the emissivities are dynamically retrieved from MHS observations at 89, 157 and 190.311 GHz.

For MHS, the variation of the emissivity spectra over sea ice needs to be taken into account when adapting the dynamic emissivity method. Figure 11 shows an example of two emissivity spectra for different types of sea ice where the emissivities are dynamically retrieved from MHS observations at 89, 157 and 190.311 GHz (i.e. channel 1, 2 and 5). The differences between the retrieved emissivities differ over different surfaces.

3.1 Assimilation experiment setup

Dynamic emissivities over land are retrieved for AMSU-A and MHS sounding channels respectively at 50.3 GHz (i.e. channel 3) and at 89 GHz (i.e. channel 1). We will refer hereafter to the channels with this role as emissivity channels.

The dynamic emissivity scheme has been adapted for sea-ice conditions as follows: for AMSU-A, we apply the same scheme that is used over land, as the AMSU-A sounding channels are close enough in frequency to the emissivity channel used. For MHS, the low resolution experiments showed that the usage of emissivities retrieved at 157 GHz performs better than applying the same channel that is used over land. This is confirmed by the scatter plots in Figure 12 showing emissivities retrieved at channel 1 frequencies (89 GHz, left) and channel 2 frequencies (157 GHz, right) versus emissivities retrieved at channel 5 frequencies (190.3 GHz). Following these results, we test here only emissivities retrieved from channel 2 to be used for the simulation of the water vapour channels channel 3 and 4, while we do not activate the assimilation of MHS channel 5 over sea ice. Departure statistics show too large remaining biases for MHS channel 5, given the strong sensitivity to the surface as a result of its weighting function moving down in the atmosphere as the water vapour decreases with the latitude.

Data over sea are simulated everywhere with FASTEM emissivities (Liu et al. 2011).

Table 1 and 2 summarise the usage of ASMU-A and MHS channels over land, sea and sea ice, indicating also the role of the quality control channels (one stage of the quality control for clear-sky observations at ECMWF is performed applying a threshold to the first-guess departures of window channels in order to detect cloud/rain contamination). Entries in bold font in the tables indicate changes in the experiments that we have run compared to the operational usage.

To take into account the variation of the emissivity spectra over sea ice, we have tested two different corrections for the emissivities of the MHS quality control channel (channel 1), both based on the brightness temperature difference between channel 2 (TB_2) and 1 (TB_1).

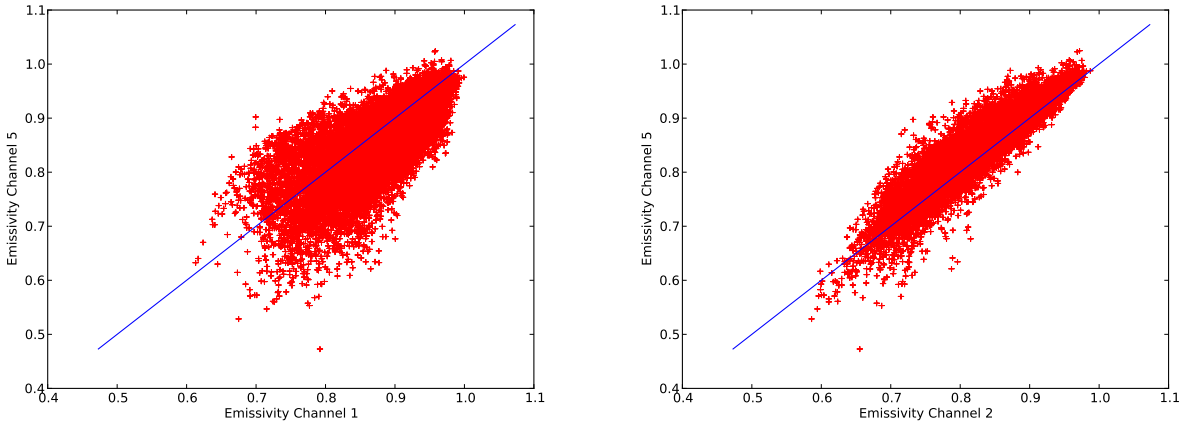

Figure 12: Dynamic emissivities for MHS over sea ice retrieved at channel 1 frequencies (89 GHz, left) and channel 2 frequencies (157 GHz, right) versus emissivities retrieved at channel 5 frequencies (190.3 GHz).

We have tested the correction term currently used in the Meteo France system (Bouchard et al. 2010), i.e.:

$$\begin{aligned} \varepsilon_{corrected} &= \varepsilon_{retrieved} + (TB_2 - TB_1)/TS + 0.01 \quad \text{if} \quad (TB_2 - TB_1)/TS > 0 \\ \varepsilon_{corrected} &= \varepsilon_{retrieved} + (TB_2 - TB_1)/TS + 0.02 \quad \text{if} \quad (TB_2 - TB_1)/TS \leq 0 \end{aligned} \tag{1}$$

and a correction term that varies with the size of retrieved emissivity as follows:

$$\varepsilon_{corrected} = \varepsilon_{retrieved} + (TB_2 - TB_1)/TS + \exp(-4.5\varepsilon_{retrieved}) \tag{2}$$

Both corrections have been derived empirically, based on relationships such as the ones shown in Figure 12. We refer hereafter to these corrections as the MF correction (equation 1) and the exponential correction (equation 2), and to the experiments performed as the sea ice experiments (though we are also enhancing the coverage of data over sea).

Figure 13 shows the scatter plots of emissivities retrieved from channel 1 and emissivities retrieved from channel 2 corrected with the MF correction (left) and the exponential correction (right) in the summer season. The exponential correction gives, on average, larger emissivity values, in better agreement with the emissivities retrieved for channel 1. Therefore it provides more accurate emissivities for the quality control channel than the MF correction. This is the case also in the winter season.

Table 1: AMSU-A settings for the assimilation experiments on the enhanced use of observations at high latitudes

AMSU-A channel	land (low orography)	sea	sea ice
3	emissivity channel	quality control channel	**emissivity channel**
4	quality control channel	-	quality control channel
5	actively assimilated	actively assimilated	actively assimilated north of 60S
6-14	actively assimilated	actively assimilated	actively assimilated

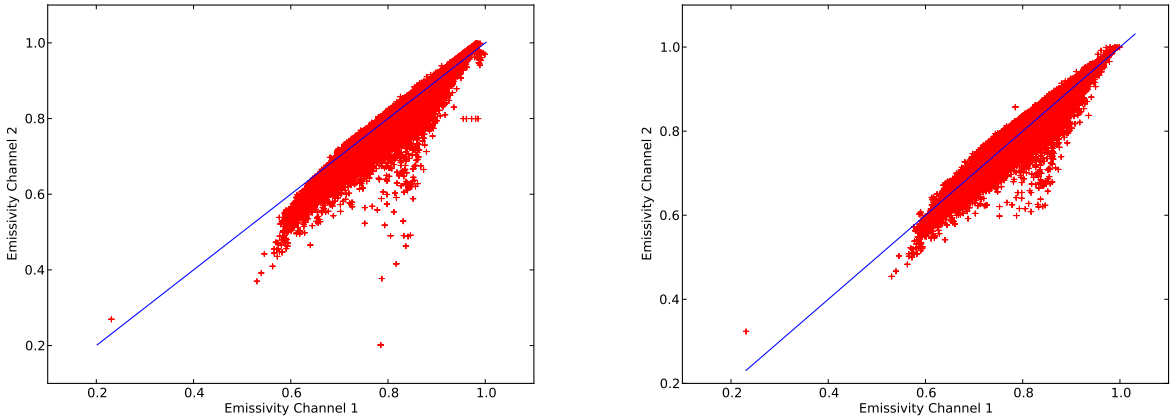

Figure 13: Dynamic emissivities retrieved from channel 1 (89 GHz) versus emissivities retrieved from channel 2 (157 GHz) corrected with the MF correction (left) and the exponential correction (right) in the summer season.

We have run three month long assimilation experiments in two seasons of 2012: summer (June, August, September) and winter (January, February, March), using the operational cycle CY38R1. The control experiment uses the static emissivity scheme for sea ice described in Kelly and Bauer (2000), and does not assimilate MHS data over surfaces with a skin temperature less than 278 K. The sea ice experiments use the dynamic emissivity scheme over sea ice as described above, and adds the assimilation of MHS channels over sea ice and cold sea surfaces as summarised in Table 2. The sea ice experiments include also some minor changes in the code related to the rejection of observations when dynamic emissivities are not feasible, and to the thresholds used to discriminate land, sea and sea ice (in order to have a more uniform treatment across the code). Table 3 summarises the experiments run in the two seasons.

3.2 Results

Here we discuss the results of the sea ice experiments versus the control in the summer and in the winter season. We will show initially the results for the experiments with correction in equation 1. Secondly, we will highlight the differences between the experiments with the two types of corrections.

The sea ice experiments show a general increase in the number of microwave sounder observations assimilated at high latitudes (see for example Figure 14). This is the case for MHS channel 3 and 4, but also for AMSU-A channel 5 to 8. While for MHS the increase in the number of used data is due to removing over sea and sea ice the constraint currently used in operations on the skin temperature (observations over surfaces with

Table 2: MHS settings for the assimilation experiments on the enhanced use of observations at high latitudes

MHS channel	land (low orography and TS$\geq$278 K)	sea	sea ice
1	emissivity channel	-	**quality control channel**
2	quality control channel	quality control channel	**emissivity channel**
3-4	actively assimilated	**actively assimilated**	**actively assimilated**
5	actively assimilated	**actively assimilated**	-

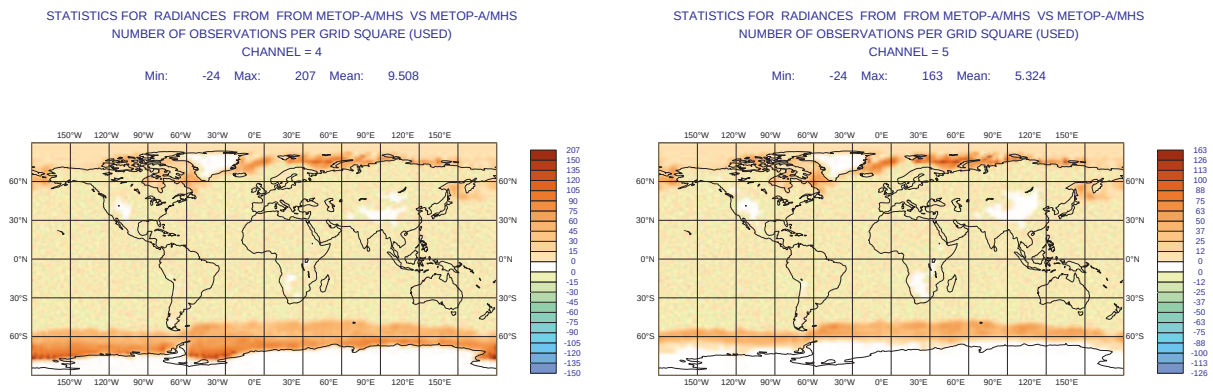

Figure 14: Count differences for MHS channel 4 (left), channel 5 (right) observations per grid box used in the atmospheric analysis between the sea ice experiment and the control experiment in one month in the summer.

skin temperature TS<278K are rejected), for AMSU-A this happens because a greater number of observations passes the quality control.

3.2.1 Departure statistics

Here we measure the impact of the AMSU-A and MHS data at high latitudes, as treated in the sea ice experiments, on the quality of the analysis and of the first guess. Figure 15 shows the histograms of first-guess departures for MHS channel 4 (left) and for AMSU-A channel 5 (right) for data over sea ice in the sea ice experiment (sky blue) and in the control experiment (red). For both sensors the dynamic emissivities lead to improved simulations for the actively simulated channels. This is the case also for other active channels: MHS channel 3 and AMSU-A channel 6. The histograms include statistics for all data, i.e. before any bias correction and quality control (the two different emissivity corrections for MHS channel 1 therefore do not play a role here). The departures of the actively assimilated data are smaller than in these histograms.

The new or better modelled observations change the temperature analysis field over sea ice. For the summer season, these changes are greater over the South Pole, while in the winter season the effect of the modifications over sea ice is seen both in the South and North Pole. Figure 16 shows the 850 hPa temperature differences between the sea ice experiment and the control during the winter period. In the both seasons a warming of circa 0.5 K occurs in the South Pole (a similar change is observed at 1000 hPa), while there is only a very small cooling of circa 0.1 K of the temperature at 500 hPa. There are no relevant differences for temperatures

Table 3: Assimilation experiments on the enhanced use of observations at high latitudes

Description	ID (summer)	ID (winter)
sea ice experiment with the MF correction	fsw3	fsfb
sea ice experiment with the exponential correction	ft4e	ft4f
control experiment	fsw2	fsej

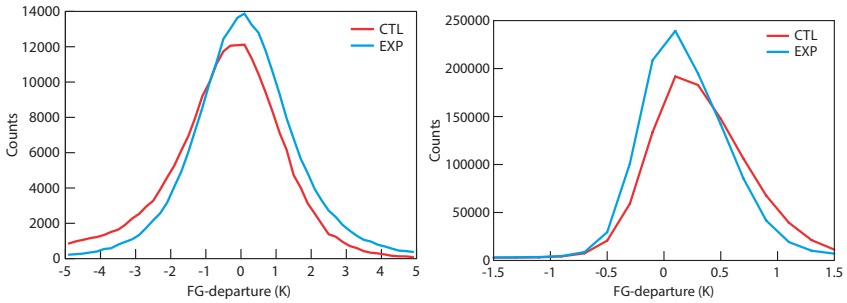

Figure 15: Histograms of first-guess departures for MHS channel 4 (left) and AMSU-A channel 5 (right) over sea ice in the summer of 2012 when emissivities are estimated by a static scheme (control experiment, red) or are retrieved dynamically from observations (sea ice experiment, sky blue). The histograms are based on departures before bias correction and before cloud screening has been applied.

at higher levels. Observation statistics partly support these changes to the mean analysis: the fit to radiosonde temperature measurements in the South Pole region shows that the sea ice experiment is reducing the bias in the analysis at around 850 hPa, bringing the anlysis in better agreement with the radiosondes (see Figure 17). Note, however, that the largest changes to the mean temperature analysis occur in areas not sampled by these radiosondes.

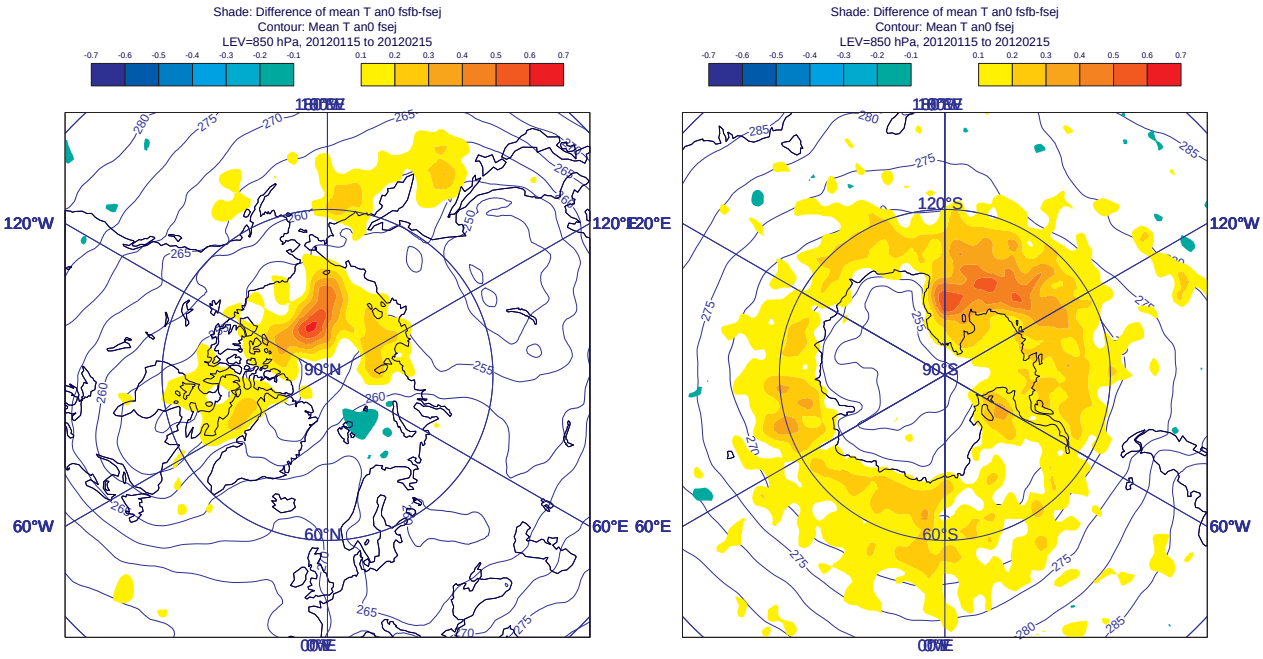

Figure 16: Mean temperature analysis differences at 850 hPa in the North Pole (left) and south Pole (right) between the sea ice experiment and the control in K in the winter season . Contour lines represent mean temperature analysis in the control experiment.

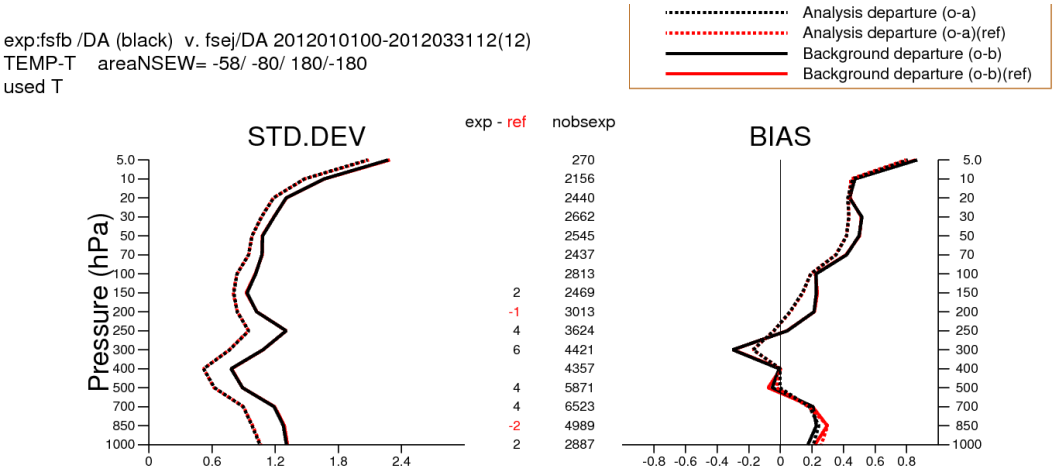

Figure 17: Radiosonde temperature departure statistics for the sea ice experiment in the winter season (black) and the control experiment (red) for an area of South Polar Circle.

The sea ice experiment makes the humidity field wetter at 850 and 700 hPa compared to the control experiment (the difference in relative humidity are up to 10.5 %). The fit to radiosonde measurements in the South Pole show that both experiments have a negative bias toward the observations at 850 and 700 hPa (the model fields are too dry) and the sea ice experiment is consistently reducing this bias (see for example Figure 18) in both seasons.

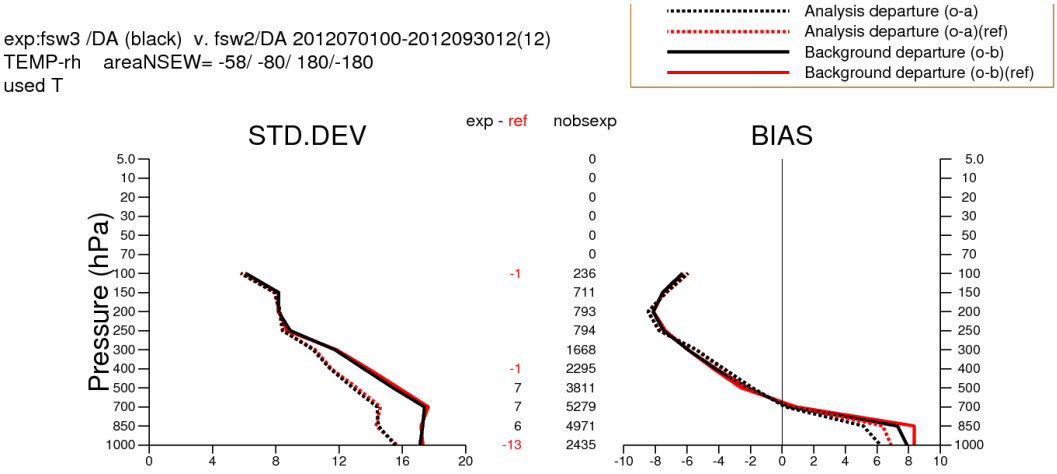

Figure 18: Radiosonde relative humidity departure statistics for the sea ice experiment in the summer season (black) and the control experiment (red) for an area of South Polar Circle.

The experiments with the correction as in equation 2 show similar statistics in terms of fit to radiosonde observations. The only relevant difference between the experiments using a different correction for the MHS quality channel is in the impact of the low level temperature analysis field in the winter season. The sea ice experiment with the exponential correction is slightly cooler at 1000 hPa in the North Pole than the experiment with the MF correction. However radiosonde statistics do not show relevant differences between the two corrections.

3.2.2 Forecast impact

Forecast results are computed for different variables and regions for 92 days (summer) and 91 days (winter) of the assimilation experiments described above. The sea ice experiment run in the summer season with the MF correction shows a positive impact for the forecast of the temperature, geopotential and winds in the Southern Hemisphere, and an impact mainly neutral elsewhere. The winter experiment shows a positive impact for the relevant atmospheric variables in both hemispheres, which is in agreement with changes in the temperature and humidity analysis fields that occur both in the North and South Polar Circles. The normalised differences in the root mean square (RMS) forecast error between the sea ice experiment and the control experiment for the forecast of the geopotential in the summer and winter season are shown in Figure 19 and Figure 20. Blue shadings indicate that the sea ice experiment has a smaller RMS error than the control experiment.

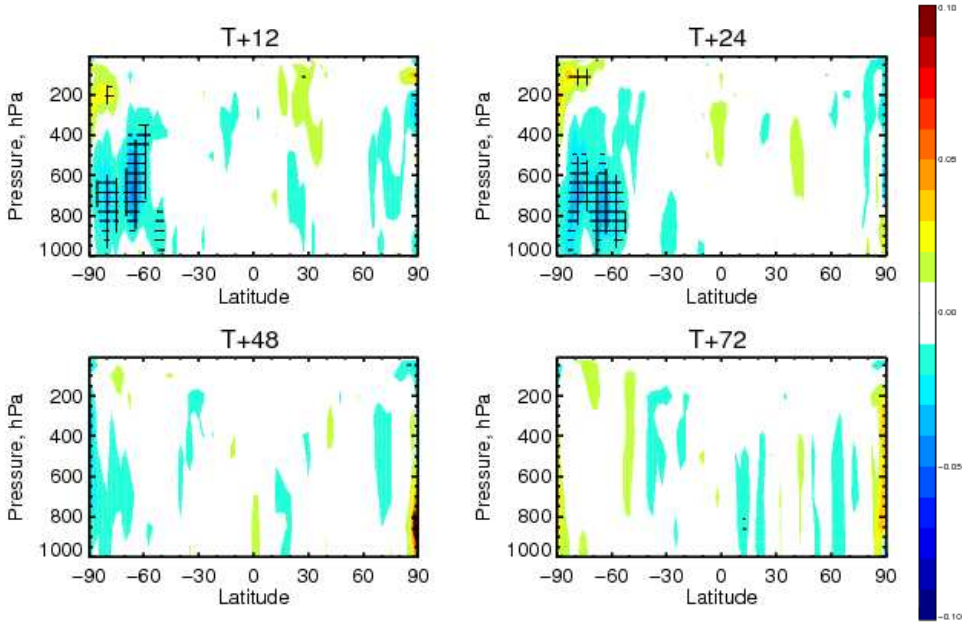

Figure 19: Normalised differences in the root mean square forecast error between the sea ice experiment (fsw3) and the control experiment (fsw2) in the summer season (July to September 2012) for the 0Z forecast of the geopotential at different pressure levels. Verification is against the experiment own-analysis.

The experiment run with the exponential correction shows similar results to the ones obtained with the MF correction with the exception of some of the scores in the winter season in the Northern Hemisphere, and in the summer season in the Southern Hemisphere. A statistically significant negative impact is observed for the forecast of the temperature and geopotential at day 9 and 10 in the Northern Hemisphere in the winter season when the exponential correction is used for the quality control channel. On the other hand, the results for the forecast of the temperature, geopotential and winds in the summer season are slightly better when using the exponential correction rather than the MF correction. On balance, it was decided to proceed with the MF correction for the operational implementation of the sea-ice emissivity scheme.

3.3 Conclusions

We have tested an enhanced assimilation of AMSU-A and MHS observations at high latitudes. A considerable number of humidity and temperature observations have been assimilated in data-sparse areas of the globe with

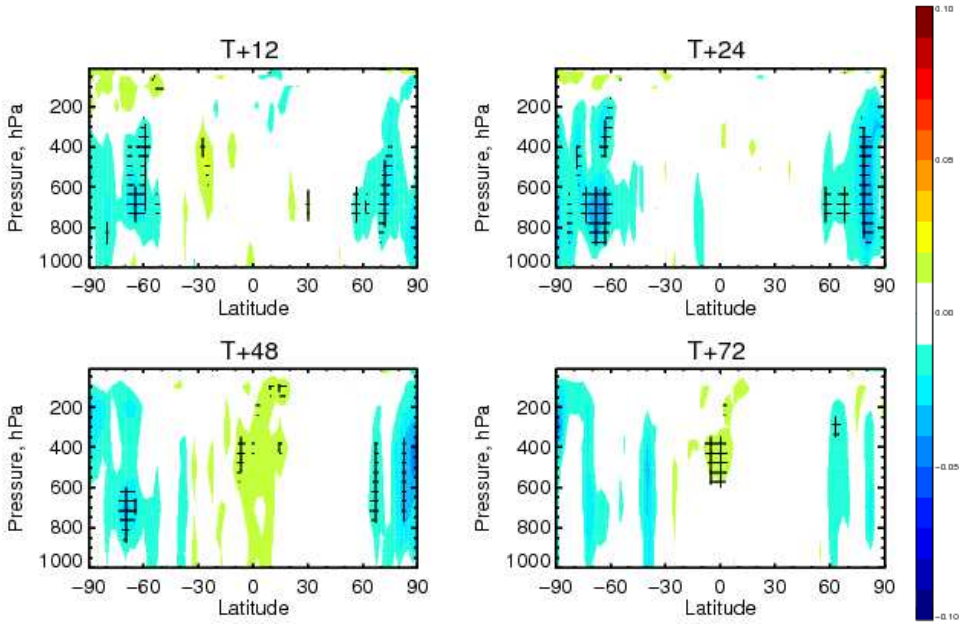

Figure 20: Normalised differences in the root mean square forecast error between the sea ice experiment (fsfb) and the control experiment (fsej) in the winter season (January to March 2012) for the 0Z forecast of the geopotential at different pressure levels. Verification is against the experiment own-analysis.

a significant impact on forecast of all relevant atmospheric variables. These results improve the outcome of low resolution experiments that were previously run to test the assimilation of observations at high latitudes.

These changes for AMSU-A and MHS described in this section have been successfully tested also for operational implementation at ECMWF in the next cycle upgrade (CY39R1), and the MF correction has been selected for the final implementation.

4 Error model for surface-sensitive observations

The observation error for AMSU-A and MHS is expressed in the ECMWF assimilation system by a diagonal covariance matrix wich is currently globally constant. However, this observation error should also include the forward model error, and this error contribution varies greatly with the surface characteristics and the viewing geometry for observations that are sensitive to the surface. In particular, the error in the surface emissivity varies considerably with surface type. Furthermore, for a given channel the sensitivity to the surface varies along the scan line. AMSU-A and MHS observe the Earth at different viewing angles from nadir (due to their cross-scanning capability), resulting in different sensitivity to the surface: observations at outer scan positions are less sensitive to the surface than nadir ones as the atmospheric path increases away from nadir.

As shown in the second year fellowship report, standard deviations of first-guess departures increase with increasing sensitivity to the surface (increasing transmittance τ) as errors in the modelling of the surface emission become more relevant (English 2008). Figure 21 shows binned standard deviations of first-guess departures for AMSU-A channel 5 for data over land not rejected by quality control (i.e. clear-sky data). This motivates the introduction of a situation-dependent observation error.

The studies in the section will focus on characterising a situation-dependent observation error for AMSU-A

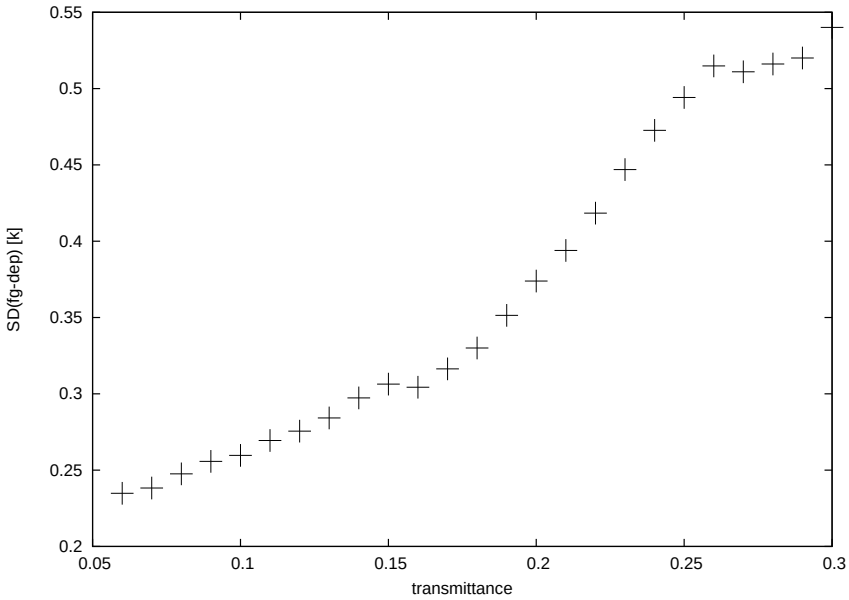

Figure 21: Mean values of standard deviations of first-guess departures for AMSU-A channel 5 in a 0.01 transmittance bin for clear-sky data over land.

channel 5. Channel 5 is the lowest peaking among the actively assimilated AMSU-A channels at ECMWF and it therefore shows the largest sensitivity to the surface and the related forward model errors.

4.1 Assimilation experiment setup

In the following, we consider the following model for the observation error σ_O for AMSU-A channel 5:

$$\sigma_O = \sqrt{0.25^2 + TS^2\ \tau^4\ \sigma_\varepsilon^2} \tag{3}$$

Here, TS is the surface skin temperature, τ the total surface-to-space transmittance, and σ_ε the error in the surface emissivity. The model above is a simplified version of the error analysis derived in English (2008), with the error in the skin temperature not explicitely expressed. In the ECMWF system a sink variable for skin temperature is used among the control variables to account for errors in the skin temperature, so contributions to the skin temperature error should not be included in the specified observation error.

We use different values for the surface emissivity error σ_ε for different surface types. These types have been chosen to broadly reflect our different ability to estimate surface emissivity. The classification used has been based on the values of albedo, skin temperature, land-sea mask, snow and sea ice products (see Figure 22 for an example). The estimates of emissivity errors for the six different surface types are in Table 4, together with examples for corresponding values of observation errors for AMSU-A channel 5 near nadir (with transmittance τ=0.15) and near the edge of the scan (with τ=0.1), estimated for a skin temperature TS=280K. The estimates for σ_ε have been derived from estimates for the typical uncertainty in the dynamic emissivity retrievals, together with fitting the $TS^2\ \tau^4\ \delta\varepsilon^2$ term to relationships between standard deviations of FG-departures as a function of τ. Examples of the transmittance-dependent statistics used for the latter calculations are in Figure 23 for two different surface types.

We have run a preliminary assimilation experiment where the observation error for AMSU-A channel 5 is surface-dependent as in equation 3 and the emissivity errors are as in Table 4. Figure 24 shows the observation

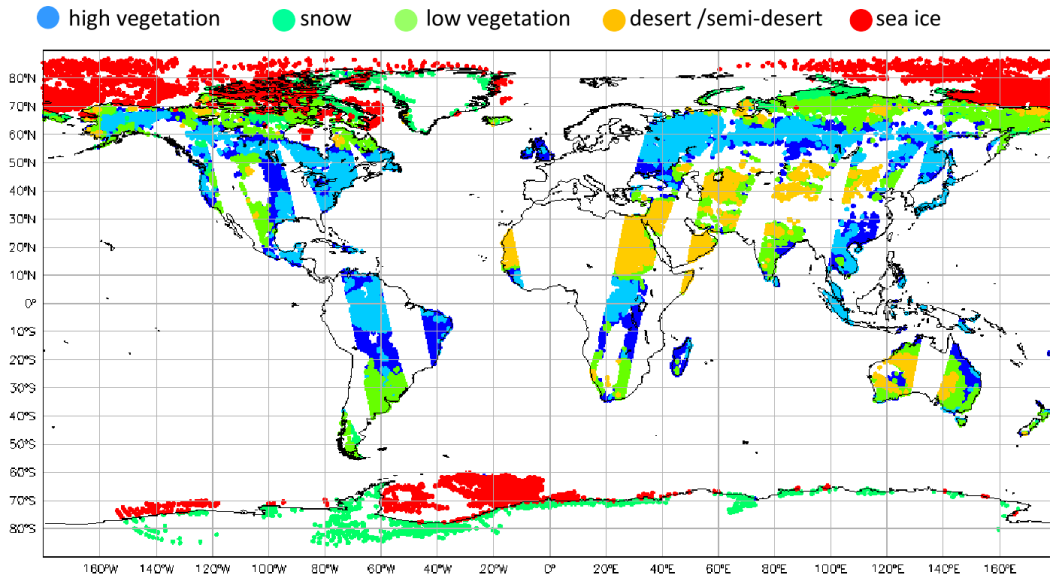

Figure 22: Surface classification of land and sea ice associated to a 12 hour observation window of AMSU-A Metop-A. The classification is based on observational database fields (dark blue land is not classified by the scheme used).

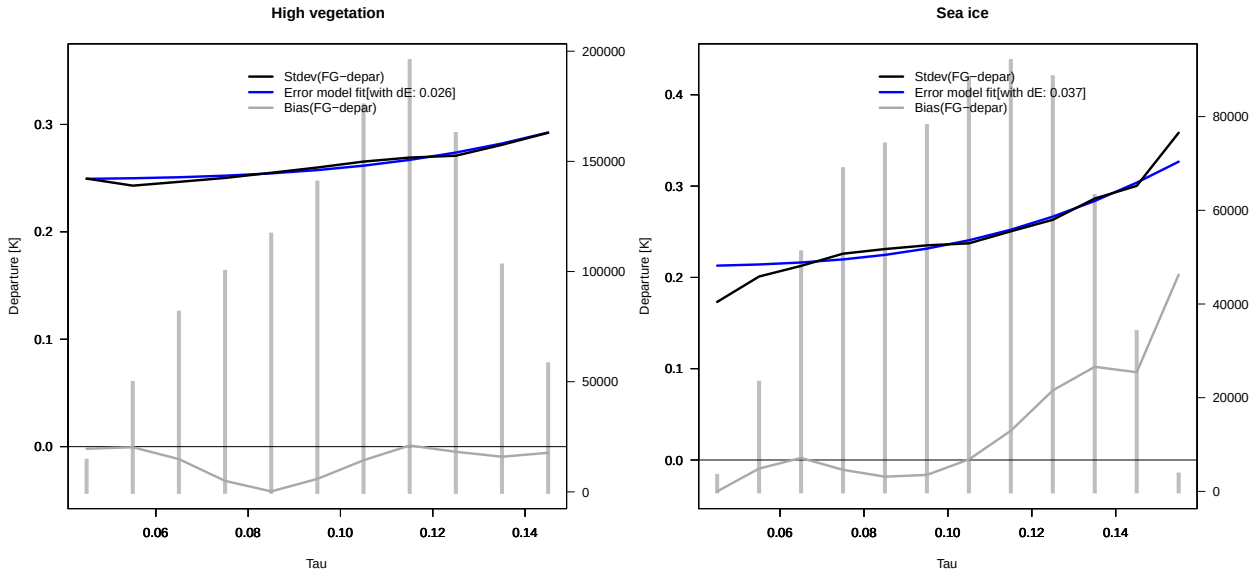

Figure 23: Mean values of standard deviations of first-guess departures and bias for AMSU-A channel 5 onboard Metop-A, NOAA-15, -18, and -19 in a 0.02 transmittance bin, and error model fit (in blue) over high vegetation (left) and sea ice (right). Also shown is the number of observations used per bin (right-hand axis). First-guess departures are considered after some quality control based on first-guess checks applied to a lower channel. The three outermost scan positions are also disregarded in the calculations. For the high vegetation case, first-guess departures are considered for observations with a transmittance lower than 0.15 (so not to include data with a large bias over high orography).

error for AMSU-A channel 5 on Metop-A for a 12 hour observation window. The significant dependence of the observation error on the scan-position is clearly visible, as is the contrast between land and sea. Regions of high orography show the largest observation errors, as channel 5 shows the strongest sensitivity to the surface here.

The control experiment uses the same observation error for AMSU-A channel 5 as it is used in the operational configuration, i.e. a global value equal to 0.28 K for the diagonal element of the error covariance matrix. We refer hereafter to the above experiments as the observation error experiment and the control experiment. The experiments were run at a T511 resolution with the ECMWF cycle CY38R1 for July, August and September 2012.

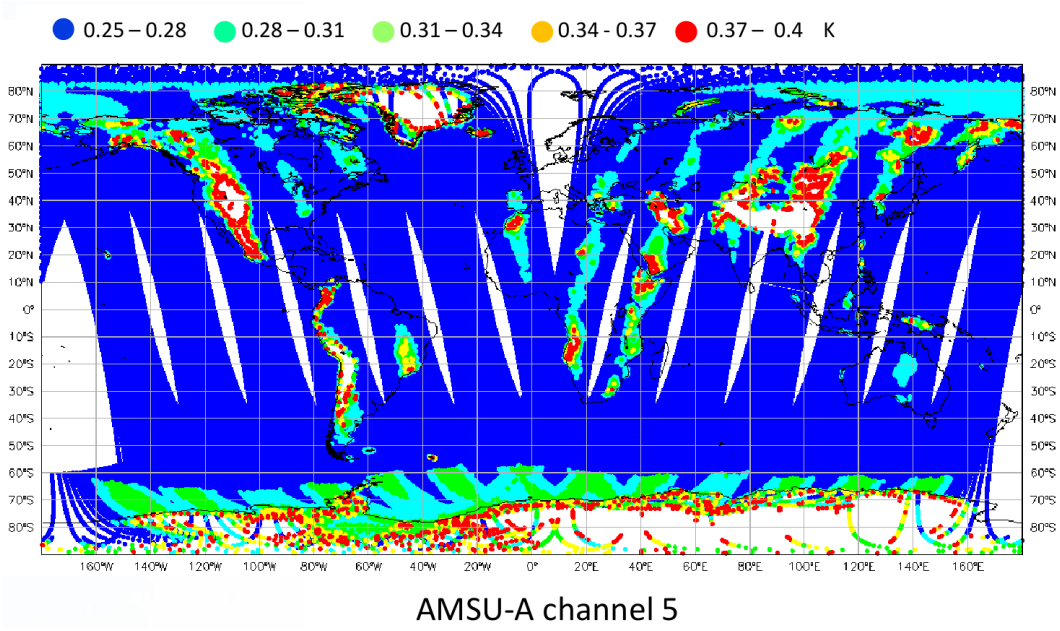

Figure 24: Observation error estimates for AMSU-A channel 5 on Metop-A for a 12 hour observation window.

4.2 Results

There are no relevant differences between the first-guess deparure statistics of the observation error experiment and the control. In particular, the new observation error does not change significantly the fit to AMSU-A channel 5 over the different surfaces (see Figure 25). Analysis departures for AMSU-A channel 5 show a slightly better fit to observations in the observation error experiment than in the control, both over land and over sea (see Figure 26). This latter result is expected given the usage of a smaller observation error in the observation error experiment than in the control for observations away from nadir.

Table 4: Estimates of surface-dependent observation errors for AMSU-A channel 5

surface type	emissivity error	observation error near nadir	observation error near the scan edge
high vegetation	0.026	0.30	0.26
low vegetation	0.030	0.31	0.26
desert/semidesert	0.024	0.29	0.26
snow	0.041	0.36	0.27
sea ice	0.037	0.34	0.27
sea	0.008	0.25	0.25

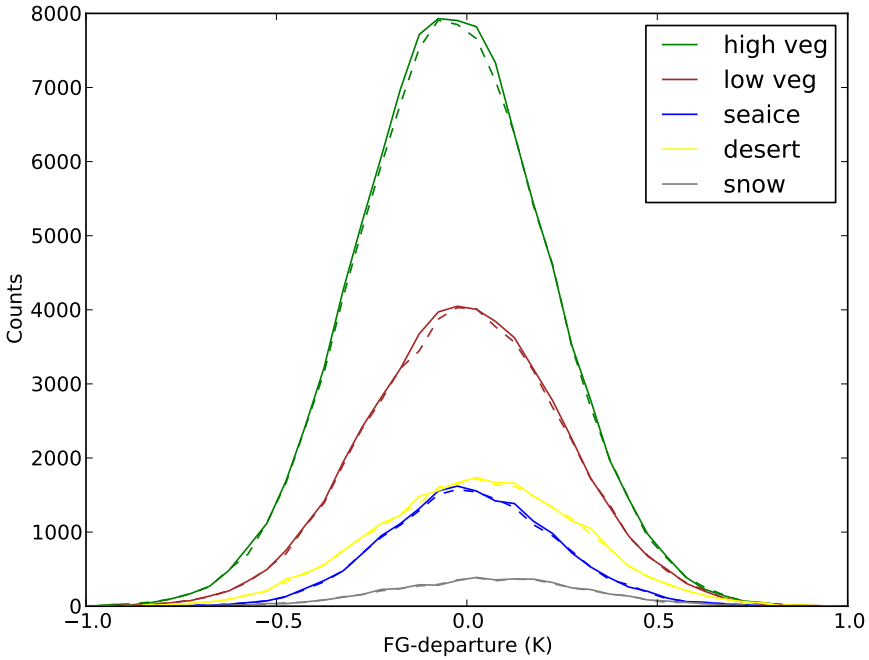

Figure 25: Histograms of first-guess departures for Metop-A AMSU-A channel 5 over high vegetation, desert, snow, low vegetation and sea ice in the control experiment (dashed line) and the observation error experiment (solid line). Histograms are based on one month departures of actively assimilated data.

Forecast results are computed for different variables and regions for 92 days of the assimilation experiments described above. The scores of temperature, geopotential, winds and humidity are not statistically significantly different between the observation error experiment and the control. This is consistent with the small changes observed in the departure statistics of the two experiments. However, differences in the root mean square forecast error for temperature at 850 hPa at time $T + 12$ between the two experiments show smaller errors over sea in the observation error experiment compared to the control experiment (see Figure 27). This gives an indication of smaller analysis increments over sea when a smaller observation error is used, and hence of a better consistency between the short-range forecast and the observations.

4.3 Conclusions

We have estimated a surface-dependent observation error for AMSU-A channel 5, the lowest peaking channel among the actively assimilated AMSU-A channels at ECMWF. The error takes into account both the observation sensitivity to the surface and the emissivity errors as it is dependent on the channel transmittance from surface to space and on the type of surface observed (high vegetation, low vegetation, desert/semidesert, snow, sea ice and sea). The estimated observation errors are smaller than what is currently used in operations for AMSU-A channel 5 near the scan edge, and are bigger (with the exception of sea surfaces) for observations near nadir.

We have tested the new observation error model in preliminary assimilation experiments run at a T511 resolution. The assimilation trials show a neutral impact from using situation-dependent observation errors compared

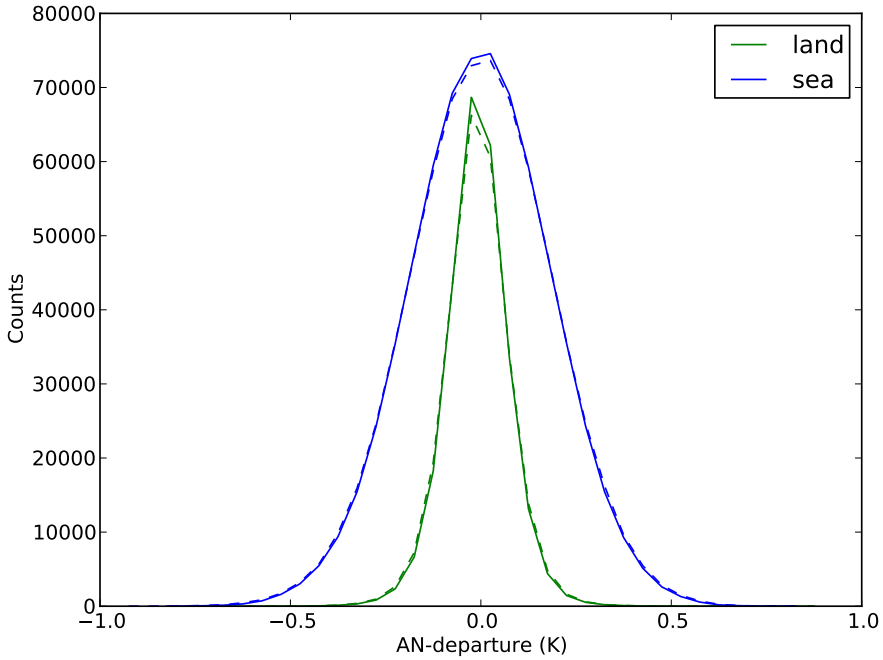

Figure 26: Histograms of analysis departures for Metop-A AMSU-A channel 5 over land and sea in the control experiment (dashed line) and the observation error experiment (solid line). Histograms are based on one month departures of actively assimilated data.

to the globally constant value of 0.28 K. This study provides an initial base for future work towards a more efficient usage of surface-dependent observations. Refinements of the observation error formulation may be necessary. Also, the situation-dependent observation errors may allow an extended use of AMSU-A channel 5, for instance over sea ice in the Southern Hemisphere where it is currently blacklisted. This is left for future work.

5 General conclusions

This study investigates a general enhancement of the usage of satellite microwave observations at ECMWF. Here we briefly summarise the main findings of this work.

The quality of the microwave sounder data from the recently launched Metop-B satellite has been evaluated through a comparison with simulated radiances from the model state. Statistics of first-guess departures show that both AMSU-A and MHS sensors are in very healthy conditions. As result of these studies the two Metop-B microwave sounders have been actively assimilated at ECMWF since 10 December 2012.

We have tested an enhanced assimilation of AMSU-A and MHS observations at high latitudes. A considerable number of humidity and temperature observations have been assimilated in data-sparse areas of the globe with a significant impact on forecast of all relevant atmospheric variables. These changes will be implemented at ECMWF in the next cycle upgrade (CY39R1).

We have estimated a surface-dependent observation error for AMSU-A channel 5 (the lowest peaking channel

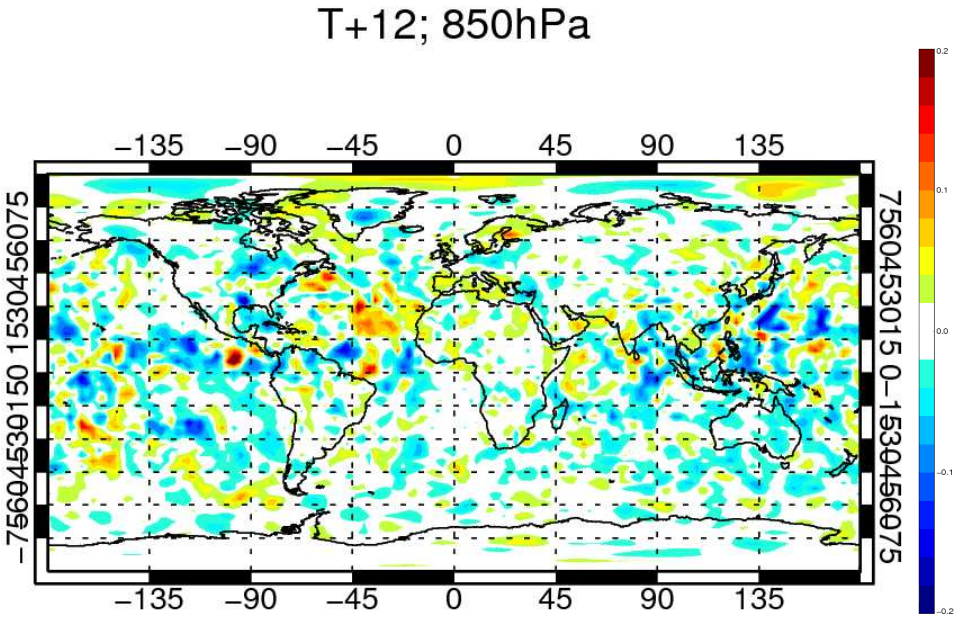

Figure 27: Map of the differences in root mean square forecast error between the observation error experiment and the control for the 0Z forecast of the 850 hPa geopotential at T+12, calculated over the whole experiment period. Verification is against experiment own-analysis.

among the actively assimilated AMSU-A channels at ECMWF) which takes into account the observation sensitivity to the surface and the emissivity errors of different types of surfaces. This study provides an initial base for future work towards a more efficient usage of surface-dependent observations.

Acknowledgements

Enza Di Tomaso is funded by the EUMETSAT Fellowship Programme. Alan Geer is thanked for his help in this work. Anabel Bowen and Rob Hine are gratefully acknowledged for their help editing some of the figures.

References

Bouchard, A., F. Rabier, V. Guidard, F. Karbou (2010), Enhancements of Satellite Data Assimilation over Antarctica, Monthly Weather Review, 138(6), 2149-2173.

Di Tomaso, E. and N. Bormann (2012),Assimilation of ATOVS radiances at ECMWF: second year EUMETSAT fellowship report, EUMETSAT/ECMWF Fellowship Programme Research Report No 26, August 2012.

Di Tomaso, E. and N. Bormann, Assimilation of ATOVS radiances at ECMWF: first year EUMETSAT fellowship report, EUMETSAT/ECMWF Fellowship Programme Research Report No 22, March 2011.

English, S. J. (2008), The Importance of Accurate Skin Temperature in Assimilating Radiances From Satellite Sounding Instruments. IEEE Transactions on Geoscience and Remote Sensing, 46(2), 403-408.

Karbou, F., E. Grard, F. Rabier (2005), Microwave land emissivity and skin temperature for AMSU-A and -B

assimilation over land. Q. J. R. Meteorol. Soc., 132, 2333-2355.

Kelly, G. and Bauer, P. (2000), The use of AMSU-A surface channels to obtain surface emissivity over land, snow and ice for numerical weather prediction, In Proceedings of 11th International TOVS Study Conference, Budapest, Hungary, 167-179.

Liu, Q., F.Weng and S.J. English (2011), An Improved Fast Microwave Water Emissivity Model. IEEE Trans. Geosci. Remote Sens., 49, 1238-1250.

Microwave Instruments (2012), Available at:

http://www.ecmwf.int/products/forecasts/d/charts/monitoring/satellite/mwimg/ (Accessed: 06 Dec 2012).